FULL PAPER

On the Relation between Morphology and FET Mobility of Poly(3-alkylthiophene)s at the Polymer/SiO_2 and Polymer/Air Interface

Wibren D. Oosterbaan, Jean-Christophe Bolsée, Linjun Wang, Veerle Vrindts, Laurence J. Lutsen, Vincent Lemaur, David Beljonne, Christopher R. McNeill, Lars Thomsen, Jean V. Manca, and Dirk J. M. Vanderzande**

The influence of the interface of the dielectric SiO_2 on the performance of bottom-contact, bottom-gate poly(3-alkylthiophene) (P3AT) field-effect transistors (FETs) is investigated. In particular, the operation of transistors where the active polythiophene layer is directly spin-coated from chlorobenzene (CB) onto the bare SiO_2 dielectric is compared to those where the active layer is first spin-coated then laminated via a wet transfer process such that the film/air interface of this film contacts the SiO_2 surface. While an apparent alkyl side-chain length dependent mobility is observed for films directly spin-coated onto the SiO_2 dielectric (with mobilities of $\approx 10^{-3}$ cm^2 V^{-1} s^{-1} or less) for laminated films mobilities of 0.14 ± 0.03 cm^2 V^{-1} s^{-1} independent of alkyl chain length are recorded. Surface-sensitive near edge X-ray absorption fine structure (NEXAFS) spectroscopy measurements indicate a strong out-of-plane orientation of the polymer backbone at the original air/film interface while much lower average tilt angles of the polymer backbone are observed at the SiO_2/film interface. A comparison with NEXAFS on crystalline P3AT nanofibers, as well as molecular mechanics and electronic structure calculations on ideal P3AT crystals suggest a close to crystalline polymer organization at the P3AT/air interface of films from CB. These results emphasize the negative influence of wrongly oriented polymer on charge carrier mobility and highlight the potential of the polymer/air interface in achieving excellent "out-of-plane" orientation and high FET mobilities.

1. Introduction

The use of solution processable polymeric semiconductors for field-effect transistors (FETs) offers attractive opportunities for the production of low-cost, flexible and large area electronics.[1] Regioregular poly(3-alkylthiophene)s (P3ATs) are well-studied materials in this field and regioregular poly(3-hexylthiophene) (P3HT) in particular serves as a benchmark material in the development of new polymeric semiconductors due to its wide availability and ease of processing from solution into crystalline thin-film microstructures.[2] Hole mobilities of up to 0.1 to 0.2 cm^2 V^{-1} s^{-1} have widely been demonstrated for P3HT.[3,4] The hole mobility has been found to be largely dependent on polymer morphology, crystallinity, and crystal orientation.[5–8]

It is well established that P3ATs crystallize in a lamellar structure. The extended, (partially) flattened, and aligned thiophene backbones π-stack in the crystallographic *b*-direction, and several of these stacks with identical orientation pile up in the *a*-direction (**Figure 1**).[9,10]

In the bulk of thin P3AT films, two crystal orientations with respect to the plane of the film tend to dominate;[3,8,11] with the thiophene rings "edge-on" or "out-of-plane" (oop) and "face-on" or "in-plane" (ip) (Figure 1). It has been shown that the FET mobility for thin P3HT films with a pronounced (bulk) oop orientation is ≈100 times higher than for films with ip oriented crystals.[3] The crystal orientation as found in the bulk, however, is

Dr. W. D. Oosterbaan, Dr. J.-C. Bolsée,
Prof. J. V. Manca, Prof. D. J. M. Vanderzande
Hasselt University
Campus Diepenbeek, Institute for Materials Research
Agoralaan Building D, 3590, Diepenbeek, Belgium
E-mail: wibren.oosterbaan@gmail.com;
dirk.vanderzande@uhasselt.be
Dr. L. Wang, Dr. V. Lemaur, Dr. D. Beljonne
Laboratory for Chemistry of Novel Materials
University of Mons
Place du Parc 20, B-7000, Mons, Belgium

DOI: 10.1002/adfm.201303298

Dr. C. R. McNeill[+]
Optoelectronics Group, Cavendish Laboratory
University of Cambridge
J J Thomson Ave, Cambridge, CB3 0HE, UK
Dr. L. Thomsen
Australian Synchrotron
800 Blackburn Road, Clayton, Vic-3168, Australia
V. Vrindts, Dr. L. J. Lutsen, Prof. J. V. Manca, Prof. D. J. M. Vanderzande
IMEC-IMOMEC
Wetenschapspark 1, 3590, Diepenbeek, Belgium
[+]Present Address: Department of Materials Engineering,
Monash University, Wellington Road, Clayton, Victoria, 3800, Australia

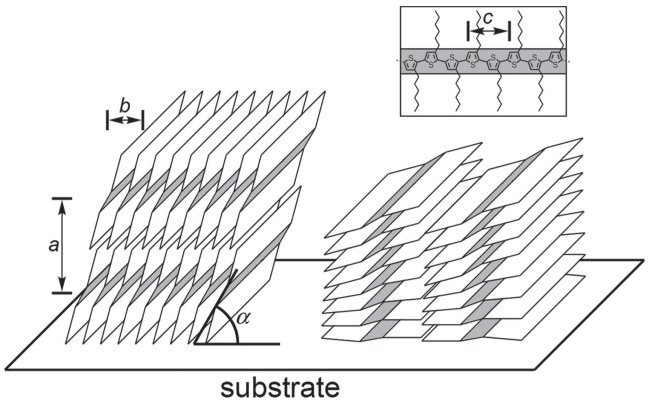

Figure 1. Schematic of the two predominant P3*A*T crystal orientations with the thiophene rings oriented "out-of-plane" (left) and "in-plane" (right). Indicated are the directions and unit cell dimensions of the crystallographic axes *a*, *b*, and *c* and the thiophene tilt angle α.

not necessarily identical to that at the interface with the gate dielectric, where the accumulation layer is located. In fact, proper interface engineering of the gate dielectric can lead to significantly enhanced FET mobilities.[12,13] It has been found, for example, that the FET mobility of P3HT increases with lowering the surface energy of the gate dielectric on which the layer is deposited,[14,15] while specific interactions with polar groups can enhance the FET mobility.[16]

Well-known agents to reduce the surface energy of the SiO_2 gate dielectric are hexamethyldisilazane (HMDS) and octadecyltrichlorosilane (OTS). Their use typically leads to hole mobilities for P3HT FETs of up to ≈0.1 $cm^2\ V^{-1}\ s^{-1}$,[3] while for bare SiO_2 mobilities generally do not exceed 0.02 $cm^2\ V^{-1}\ s^{-1}$,[17–22] even after thermal annealing. It has been shown that OTS and HMDS promote the formation of large populations of highly oop oriented crystals at the gate dielectric, which in turn is believed to reduce the amount of grain boundaries thus increasing mobility.[23] The low mobility on bare SiO_2, generally observed for polythiophenes, has been attributed to the relatively large amount of unoriented polymer at the interface with SiO_2, which would constitute trapping sites.[24,25]

We have recently shown, using near edge X-ray absorption fine structure (NEXAFS) spectroscopy,[26] that the well-known[20] decrease in FET mobility with increasing alkyl chain length for P3*A*T layers spin-coated from a single solvent correlates strongly with a decrease in oop orientation of the polymer at the interface with SiO_2. This trend in the orientation was also observed in the bulk for the crystalline polymer fraction by means of selected area electron diffraction (SAED).

In contrast to films from chlorobenzene (CB), relatively high and alkyl chain length independent hole mobilities were observed for layers spin-coated from dispersions of crystalline P3*A*T nanofibers (NFs). This was found to be consistent with the high and alkyl chain length independent level of oop orientation of the polymer in the NFs at the SiO_2 gate dielectric. Still, hole mobilities as measured on untreated SiO_2 did not exceed 3.5×10^{-3} $cm^2\ V^{-1}\ s^{-1}$.[26] Samitsu et al. have also demonstrated alkyl chain length independent hole mobilities for isolated P3*A*T NFs and NF networks on an OTS-treated SiO_2 gate.[27]

In this contribution, we extend our understanding of the relation between alkyl chain length dependent polymer microstructure and FET mobility in thin P3*A*T films to the "polymer/air" interface (although we use N_2 instead of air). Via film transfer methods it is possible to flip a polymer semiconductor film in such a way that the original polymer/air interface faces the bare SiO_2.

Film transfer methods have been used before to demonstrate that the polymer orientation at the interface is very important to charge carrier mobility. For example, Chabinyc et al. spin-coated PQT-12,[28] a polythiophene structurally similar to P3*A*Ts, on OTS-treated SiO_2, transferred the film to bare SiO_2 without flipping the film, and obtained a mobility approaching that of a layer spin-coated directly on OTS/SiO_2 (0.03 vs 0.06 $cm^2\ V^{-1}\ s^{-1}$), while PQT-12 films spin-coated directly on bare SiO_2 yielded mobilities of only ≈10^{-3} to 10^{-4} $cm^2\ V^{-1}\ s^{-1}$.[29] Until recently, the polymer/air interface was not considered to be very promising for FET applications, although top gate FETs were known to often exhibit higher mobilities than bottom gate devices. Nevertheless, Kim et al. had already demonstrated a relatively high mobility of ≈0.1 $cm^2\ V^{-1}\ s^{-1}$ for P3HT at the polymer/air interface by spin-coating a P3HT film from chloroform and flipping it such that the polymer/air interface was facing the (HMDS-treated) SiO_2 gate dielectric.[30] Recently, Wei et al.[31] demonstrated alkyl chain length independent mobilities of ≈0.05 $cm^2\ V^{-1}\ s^{-1}$ for flipped P3*A*T films measured at a BCB (Cyclotene 3000) passivated SiO_2 gate dielectric.

Here, we demonstrate alkyl chain length independent FET mobilities of 0.14 ± 0.03 $cm^2\ V^{-1}\ s^{-1}$ at the polymer/air interface of P3*A*T films spin-coated from CB by transferring these films to FET substrates with a bare SiO_2 gate dielectric. We furthermore show, using NEXAFS spectroscopy, that the polymer adopts very high levels of oop orientation at the polymer/air interface of films spin-coated from CB. By a combination of NEXAFS spectroscopy on films from CB, films from dispersions of crystalline NFs and molecular mechanics calculations, we demonstrate that the high mobilities can be attributed to the highly crystalline nature and oop orientation of the polymer at the interface with air.

Finally, we compile all our data on P3*A*T interface organization and FET mobility for P3*A*T interfaces formed at SiO_2 and air to demonstrate that the FET mobilities at the air interface are much higher than one could naively expect on the basis of increased oop interface orientation alone.

2. Results and Discussion

We will proceed using abbreviations which unambiguously indicate the number of carbons *A* in the alkyl side chain of the P3*A*Ts, such as P34T, P36T, and P38T instead of the more commonly used P3BT, P3HT, and P3OT for poly(3-butylthiophene), poly(3-hexylthiophene) and poly(3-octylthiophene), respectively.

2.1. Materials

The P3*A*Ts we used were synthesized in our laboratory via the Rieke method as described previously[32] and are of the same

Table 1. P3*A*T properties (*A* = number of carbon atoms in *n*-alkyl side chain),[32] solvents used for NF formation,[32] mass fraction f_{NF} of polymer aggregated into NFs,[32] and average FET mobilities with current on/off ratios $I_{on/off}$ and threshold voltages V_T of flipped P3*A*T film devices from layers spin-coated from CB.

Polymer [32]				NF[32]		FET (flipped films from CB)		
A	M_n [10^3 g mol^{-1}]	*PD*	*RR* [%]	Solvent used for fiber formation	f_{NF}	mobility [cm^2 V^{-1} s^{-1}]	*I* on/off	V_T [V]
4	19.5	2.29	96.5	*o*-chlorotoluene	0.94	0.0052 ± 0.0046	10^1–10^2	25 ± 6
5	16.7	1.93	94.5	*p*-xylene	0.76	0.13 ± 0.013	10^2	9 ± 5
6	23.7	1.80	94.5	*p*-xylene	0.77	0.155 ± 0.035	10^2	14 ± 5
7	24.4	1.64	97	[a]		0.11 ± 0.011	10^3	33 ± 5
8	28.0	1.66	97	pinane	0.92	0.125 ± 0.015	10^3	18 ± 10
9	25.9	1.46	98	pinane	0.82	0.175 ± 0.065	10^2–10^3	14 ± 5

[a]P37T nanofibers were not used in this study.

batches as those described in ref.[26] We note here that the variation in regioregularity (*RR* of 94.5 to ≈98%)[26] and molecular weight (M_n of 23.0 ± 4.2 kD)[26] for our polymers are likely to be sufficiently small not to cause significant variations in morphology and/or FET mobility (**Table 1**). Also the molecular weights are expected to be high enough (M_n > 15 kD) to be outside the range for which FET mobility and crystalline order (of P36T) are known[7,8,33,34] to significantly depend on molecular weight. For a discussion on both the possible influence of *RR* and MW on morphology and FET mobility we refer to our previous paper.[26]

2.2. Field-Effect Transistors

FETs were prepared by first spin-coating the polymers from 2 wt% solutions in CB on highly doped Si substrates with a thermally grown (bare) SiO_2 layer (204 nm) on top. Subsequently, these substrates were taken out of the glovebox, floated on a 40% HF solution, which dissolves the SiO_2, detaching the Si substrate from the film which remained floating. The bottom side of these films was then washed 4 times by successively transferring the film to 4 different beakers with 18 MΩ water. Finally, the films, floating on water, were taken out with a FET substrate in such a way that the former top side of the film (polymer/air interface) would face the FET structure, in effect flipping the film. The devices were then placed in the N_2 filled glovebox again and left to dry. The whole procedure outside the glovebox was performed within ≈15 min and light was excluded whenever possible. Unfortunately, we were not able to transfer NF films large enough to cover the gate of a FET structure in this way, although we managed to transfer pieces of smaller areas, large enough for NEXAFS spectroscopy. NF films are far more brittle than films from CB.

In order to check whether any of the transfer steps would affect the mobility, two types of control experiments were performed. In the first control experiment, performed for P35T, P38T and P39T, the film, floating on water, was taken out with a FET substrate in such a way that the film was not flipped. We call these films "re-applied" films. In the second type of control experiment, performed only for P38T that gives films of relatively high mechanical strength, the film was flipped twice using the standard procedure. With the first flip, the film was deposited on a fresh SiO_2/Si substrate and with the second flip it was deposited on a FET substrate. FET measurements were performed in the linear regime as described previously.[26]

The FET hole mobilities of the "re-applied" and "flipped twice" films were virtually identical to the (previously reported[26]) hole mobilities of the respective P3*A*T films that had been directly spin-coated on the FET structures (**Table 2**). The steps performed in air were found to increase the onset voltage from values of 10 to 14 V to values of over 30 V which indicates that doping occurs, most likely due to adsorption of (highly dipolar) water molecules at the SiO_2/P3*A*T interface.[35,36] The mobilities however were not noticeably affected and it is concluded that mobilities obtained via the film transfer method are directly comparable to those obtained by spin-coating directly on the substrate.

The FET characteristics of the flipped films of P34T to P39T are given in Table 1. For P3*A*Ts with 5 or more carbon atoms in the side chain, the average mobility is 0.14 ± 0.03 cm^2 V^{-1} s^{-1}, which is 2 to 3 orders of magnitude higher than the mobilities of 10^{-3} to 10^{-4} cm^2 V^{-1} s^{-1} obtained[26] for the bottom sides of identical films (**Figure 2**). For P34T, the mobilities that we measured for different transistors on a single film were quite homogeneous with an estimated error of ≈20%. The mobilities of different films however differed substantially. For the best film we measured a mobility of (1.6 ± 0.3) × 10^{-2} cm^2 V^{-1} s^{-1} with an on/off ratio of 1000 and a V_t of –7 ± 4 V, while for the

Table 2. FET mobilities of some P3*A*T films spin-coated from 2 wt% solution in CB[26] on a bare SiO_2 gate dielectric (reference) and the values that were obtained in control experiments for films that were "re-applied" and "flipped twice" (see text).

	Reference[26]	Re-applied	Flipped twice
A	mobility / 10^{-3} [cm^2 V^{-1} s^{-1}]	mobility / 10^{-3} [cm^2 V^{-1} s^{-1}]	mobility / 10^{-3} [cm^2 V^{-1} s^{-1}]
5	1.30 ± 0.15	0.88 ± 0.10	n.d.
8	0.30 ± 0.03	0.27 ± 0.03	0.32 ± 0.03
9	0.21 ± 0.02	0.26 ± 0.03	n.d.

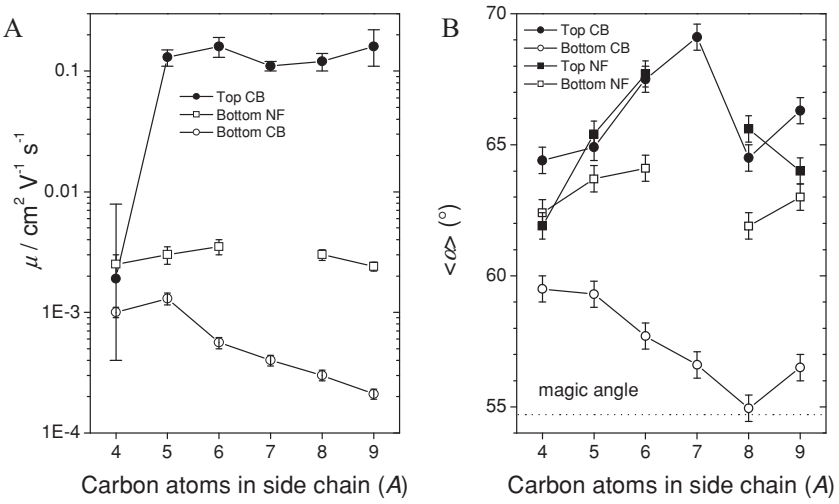

Figure 2. A) FET mobilities as a function of alkyl side chain length *A* for the flipped CB-P3*A*T films (spin-coated from 2 wt% solutions) as measured on a bare SiO_2 gate electrode. For comparison, the previously obtained[26] mobilities of the NF films and CB films spin-coated and measured on the bare SiO_2 gate dielectric are also displayed. B) NEXAFS average thiophene tilt angles <*α*> as measured for the top (air interface) of the NF- and CB-P3*A*T films. For comparison, the values previously obtained[26] for the SiO_2 interface are also displayed.

worst film it was $(9 \pm 2) \times 10^{-4}$ cm^2 V^{-1} s^{-1} (on/off ratio = 10; $V_t = 25 \pm 5$ V). A possible reason for the low and strongly varying mobility values obtained for P34T is the fact that for this polymer we are working at the solubility limit in CB. Although P34T was spin-coated from a solution cooled down from 120 °C and kept at 90 °C[26] to ensure the complete dissolution of the polymer, higher temperatures and/or lower concentrations may be needed to ensure reproducibility of film formation and higher mobility values. In the study of Wei et al.,[31] flipped films of P34T did not exhibit lower mobilities than those of P3*A*Ts with longer alkyl chains.

Note that the mobility values of 0.14 ± 0.03 cm^2 V^{-1} s^{-1} of the flipped films obtained on bare SiO_2 compare very well with state-of-the-art mobilities of 0.1 to 0.2 cm^2 V^{-1} s^{-1} obtained for similar bottom gate-bottom gold contact devices (with channel lengths > 10 μm) of P35T,[37] P36T,[4,38] and P38T[38] deposited on a HMDS and/or OTS treated SiO_2 gate dielectric and exceed previously reported values for flipped P3*A*T films.[30,31] These results suggest high levels of oop orientation[39] and crystallinity at the polymer/air interface of spin-coated P3*A*T layers,[31] similar to what has been found for the interface of P36T with a low surface energy dielectrics like OTS-treated SiO_2.[23] The alkyl chain length independent hole mobility furthermore points to a highly crystalline and fiber-like morphology at the polymer/air interface, since the mobility in P3*A*T fibers (on a bare SiO_2 gate dielectric) was also found[26] to be alkyl chain length independent (Figure 2).

2.3. Atomic Force Microscopy

In our previous study[26] we reported on the AFM results on the top (and bottom) faces of the spin-coated P3*A*T films from 1 and 2 wt% solutions in CB and on layers spin-coated from NF dispersions. For detailed AFM images, and a discussion on morphology and interface roughness we refer to sections 2.3.3 and 2.3.4 and Figures 5 and S3–S6 of that study.[26] The films from CB show both fiber-like and nodular features. The fiber widths w_{NF} for the NF layers have been determined before by the use of AFM (**Table 3** and literature).[26] For the films from CB, we extracted an average nodule width w_n from the AFM images (Table 3). The variation in w_{NF} with alkyl chain length *A* was found to be slightly larger than that in w_n. The RMS roughness of these films (over an area of 500 nm × 500 nm) decreases with increasing alkyl chain length from 7.5 to 1.1 nm, and from 4.5 to 0.6 nm for films from 2 and 1 wt% solutions in CB, respectively. Remarkably, the roughness of the P35T films from 2 wt% solutions for which we achieved mobilities of 0.13 ± 0.013 cm^2 V^{-1} s^{-1} is as high as 4.6 ± 1 nm. It is known from other poly(alkylthiophene)s, poly[5,5′]-bis(3-dodecyl-2-thienyl)-2,2′-bithiophene] (PQT-12)[40] and poly{2,5-bis(3-alkylthiophen-2-yl)thieno[3,2-*b*]thiophene}

Table 3. Average thiophene tilt angles <*α*>[a] obtained with NEXAFS at the polymer/air interface of P3AT films spin-coated on SiO_2/Si(100) from 1 wt% solutions in CB at 2000 rpm and from 0.4 to 0.6 wt% NF dispersions at 1000 rpm (see also Table 1) together with nodule widths w_n and fiber widths w_{NF} as determined with AFM for the same interfaces. For comparison, values previously reported for the SiO_2 interface[26] are also given together with values of the estimated percentage of ip oriented P3*A*T (see text).

	P3AT/Air interface				P3AT/SiO_2 interface			
	CB		NF		CB		NF	
A	<*α*> [°]	w_n [nm]	<*α*> [°]	w_{NF}[26] [nm]	<*α*>[26] [°]	ip [%]	<*α*>[26] [°]	ip [%]
	64.4	17.6 ± 3.7	61.9	14.1 ± 2.6	59.5	7.6	62.4	3.1
5	64.9	24.0 ± 5.5	65.4	22.0 ± 3.7	59.3	8.6	63.7	1.8
6	67.5	19.7 ± 3.5	67.7	27.3 ± 3.8	57.7	15	64.1	5.0
7	69.1	22.7 ± 5.0	n.d.		56.6	18	n.d.	-
8	64.5	20.1 ± 4.7	65.6	18.4 ± 3.2	55.0	15	61.9	4.0
9	66.3	22.2 ± 3.9	64.0	22.1 ± 3.5	56.5	15	63.0	5.0

[a] Estimated error: ± 0.5°.

(PBTTT),[41] that an increased roughness of the gate dielectric on which the polymer is deposited can significantly reduce the FET mobility. This was attributed mainly to reduced long range order and reduced domain sizes. In these studies, high mobilities of ≥0.1 $cm^2 V^{-1} s^{-1}$ could only be obtained for a gate dielectric with an overall RMS roughness value lower than ≈0.5 nm. The high mobilities that we obtained suggest that despite of the large roughness, relatively large and well-ordered domains are probably present at the original polymer/air interface. Although we do not expect this surface to flatten significantly on the nanometer scale (i.e., over 500 nm × 500 nm) upon contacting the SiO_2, we cannot completely exclude a contribution of such an effect to enhancing the mobility.

2.4. Polarized Near-Edge X-Ray Fine Structure Spectroscopy (NEXAFS)

In order to assess the polymer orientation at the polymer/air interface, we have measured the total electron yield (TEY) NEXAFS spectra of the carbon *K*-edge at the top sides of P3*A*T films spin-coated from 1 wt% solutions in CB (i.e., at the interface with air, which, after flipping the film, would face the gate dielectric of the FET structure). For comparison, we also performed NEXAFS spectroscopy at the top of P3*A*T layers spin-coated from NF dispersions of the same polymers (but from different solvents; see Table 1).

With NEXAFS,[42] polarized X-rays from a synchrotron are used to excite core electrons in carbon atoms of the polymer to unoccupied molecular orbitals (MOs). Especially the lowest energy, pre-ionization transition at 284.5 eV is of interest for our purpose, since it represents the excitation from the narrow 1s state to the π^* band of the polymer. This transition has a transition dipole moment that is perpendicular to the plane of the thiophene rings of the polymer[43–45] and thus can be used to extract information about the average orientation of the conjugated polymer backbone with respect to the interface. The surface sensitivity of TEY NEXAFS on regioregular P36T has been determined to be about 2.5 nm,[46] which corresponds very well with the expected depth of the accumulation layer (≈2 nm).[47] Note that, in contrast to X-ray scattering techniques, NEXAFS spectroscopy does not discriminate between crystalline and amorphous components.

Polarized NEXAFS spectra were recorded for three different angles of incidence (20, 55 and 90°) and analyzed as previously described.[26] In the analysis it is assumed that within the spot-size of the beam (0.6 mm × 0.6 mm) there is no net, long-range alignment of the polymer chains in the plane of the film.

For the top of the CB-P3*A*T layers, the analysis yielded values for the average thiophene tilt angle $<\alpha>$ with respect to the substrate plane between 64.4 ± 0.5° for P34T and 69.1 ± 0.5° for P37T (Table 3, Figure 2B). These values are much higher than magic angle (≈55°), for which no orientation preference is present, and show that at the interface with air the polymer has a pronounced oop orientation that is significantly higher than at the interface with SiO_2 for which values between 55.0 to 59.3° were previously obtained for these polymers (Table 3).[26]

The high oop orientation of 67.5 ± 0.5° for P36T is comparable to the results of Hao et al. who obtained values of 70 to 72° for P36T films spin-coated from chloroform at 400 rpm,[39] and can very well explain the high mobilities observed at the polymer/air interface. Note that the oop orientation for P36T observed by us and Hao et al. is significantly higher than the values of 59 and 60° obtained by Ho et al.[45] for layers from chloroform and CB, respectively, and also higher than the values of up to 60° that can be deduced from the data of DeLongchamp et al.[44] for layers from chloroform. These differences may in part be attributed to differences in spin-speed, solvent, *RR*, and MW (distribution).[39,45]

There are some clear differences with what was previously observed at the P3*A*T/SiO_2 interface.[26] At the polymer/air interface of the layers from CB, $<\alpha>$ follows a rather erratic course with alkyl side chain length *A*. An increase in oop orientation is observed in going from P34T to P37T, as opposed to a decrease at the P3*A*T/SiO_2 interface,[26] followed by intermediate $<\alpha>$ values for P38T and P39T. Also, in contrast to what was observed for the P3*A*T/SiO_2 interface,[26] the trend of $<\alpha>$ versus *A* is not well reflected in the mobility, which apart from P34T is independent of *A* (Table 1, Figure 2). Still, in absolute terms, the range in which $<\alpha>$ varies at the polymer/air interface is only 4.6° (64.4–69.1°), which is quite small.

Remarkably, the polymer orientation at the polymer/air interface of the NF-P3*A*T films is almost identical to that of the CB-P3*A*T films (Table 3, Figure 2B). This is in strong contrast to the orientation for both layers at the interface with SiO_2. At that interface, the NF layers have a significantly higher oop orientation than the CB layers, which is independent of *A*, while for the CB layers it decreases with *A*.[26] We can deduce from the similar widths of the fibers at the top of the NF layers (14.1 to 27.3 nm)[26] and of isolated NFs on a substrate (≈20 nm),[32] (the fiber height is only ≈5 nm)[32,48] that the orientation of the fibers with respect to the substrate for both NF layers and isolated NFs must be identical, that is, with the polymer chains (crystallographic *c*-axis) in the substrate plane and the crystallographic *a*-axis (≈alkyl chain direction) perpendicular to it. The same orientation is found in the bulk of spin-coated and drop-cast P3*A*T NF films.[32,48,49] The relative insensitivity of $<\alpha>$ to the processing conditions (CB or NF), and the fact that the (oriented) NFs are highly crystalline,[26] both suggest that α has reached a maximum value, possibly close to a crystalline value (α_{cryst}). Thus, the top of the CB-P3*A*T films is likely to be highly organized with the alkyl chains pointing out of the surface, as is the case for the NFs. This is in agreement with the findings of Hao et al. who studied the air interface of slow dried P36T layers using both polarized NEXAFS and He* Penning ionization electron spectroscopy (PIES). For (slow dried) layers with $<\alpha>$ = 70 to 72°, no ip oriented P36T could be detected with PIES, leading to the conclusion that "a near equilibrium with edge-on structure" had formed at the P36T/air interface.

The fact that the NF layers display smaller tilt angles at the interface with SiO_2 than at the interface with air can be mainly attributed to the small mass fraction ($1 - f_{NF}$) of molecularly dissolved P3*A*T in the used NF dispersions (Table 1). If it is assumed that this fraction orients like in CB-P3*A*T films both at SiO_2 and air, then tilt angles $<\alpha>_{NF/SiO2}$ for NFs at SiO_2 for most polymers can be very well predicted as: $(f_{NF}) \cdot <\alpha>_{NF/air} + (1 - f_{NF}) \cdot <\alpha>_{CB/SiO2}$, which gives 61.8, 63.6, 65.4, 64.8, and 62.7° for P3*A*Ts with *A* of 4, 5, 6, 8, and 9, respectively (measured: 62.4, 63.7, 64.1, 61.9, and 63.0°).

Until now, based on X-ray diffraction studies of Prosa et al.,[50] we tacitly assumed α_{cryst} to be close to 90° and independent of alkyl side chain length. However, our results and those of Hao et al. suggest smaller maximum setting angles which to some extend could be alkyl chain length dependent. A closer look in literature also reveals that for P36T crystals there is evidence for smaller setting angles.[51,52] In order to probe the alkyl chain length dependence of α_{cryst} and the possible occurrence of smaller values of α_{cryst} in P3*A*T crystals we performed molecular modeling simulations (vide infra).

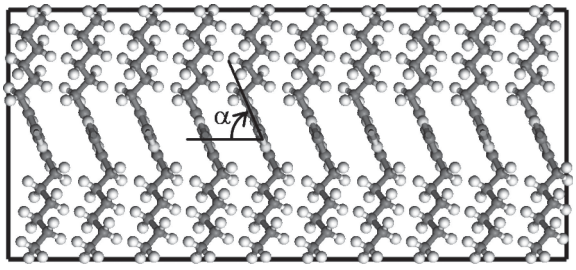

Figure 3. The optimized crystal of P36T with $\alpha = 67°$.

2.5. Theoretical Calculations

2.5.1. Molecular Mechanics Calculations

Since very similar <α> values were obtained for the top of the NF- and CB-P3*A*T films with NEXAFS, we chose to investigate the thiophene ring orientation in (ideal) crystals as a model for the surface. For this purpose, we adopted the OPLS-AA force field[53] with some of the force field parameters optimized for P3*A*Ts (see Experimental) and performed crystal energy minimizations with molecular mechanics (MM).

In the crystalline region of regioregular P34T (Form I'), P36T and P38T (both Form I) previous XRD studies indicate a lamellar packing of polymer layers in an orthorhombic primitive cell,[50,54] Since we found that our NFs are mainly composed of the Form I polymorph (with only P34T NFs containing about 50% of the more ordered Form I'),[32,55] we decided to focus on Form I/I' and not Form II, which has interdigitating side chains and a significantly larger π–π stacking distance. The crystal structure was built with an orthorhombic cell containing ten P3*A*T polymers (see **Figure 3**), each ten units long, and periodic boundary conditions were applied in all directions. In order to unravel all the possible local minima, we used different values of α (60°, 65°, 70°, ..., 120°) as starting configurations and performed full cell optimization in each case. The optimized structures fit best in a monoclinic $P2_1$ space group.

In **Table 4** we show the optimized thiophene tilt angles and their relative potential energies for all stable geometric structures, that is, those that are obtained as output from the calculations when using different initial conditions. From previous X-ray and electron diffraction studies on bulk samples, two different α_{cryst} values were obtained for P36T, namely 60°–62°[51] or 64°[52] and 85°.[50] Here, we also find two structures with close energies yet different α, 67° and 89°, in very good agreement with these previous experimental results and a recent DFT study.[56] Especially, for the geometry with α = 67°, the interlamella spacing, the intra-lamella chain-to-chain stacking distance, and the intra-chain repeated distance are calculated to be 16.8 Å, 3.8 Å, and 8.1 Å, respectively, agreeing very well with the experimental values of 16.8 Å, 3.8 Å, and 7.9 Å.[50] Note that for a molecular dynamics study of two P36T monolayers on a gate dielectric the highest oop orientation that was found equals to α = 67°.[57] For the P38T case, our data (α = 81° and 85°) also compare quite well with the experimental value, α = 84°. This holds true as well for P34T, where the calculated value of 87° is close to the value of 84°[54] determined for Form I' of P34T. Importantly, for all polymers investigated, we find stable structures with tilt angles around 67–68° and in the range 81–89°.

Table 4. The tilt angle for all the thiophene rings in the initial P3*A*T geometries (α_0), and in the optimized geometries (α), the lattice constants, the dihedral angles of S–C–C–S and C=C–C–C, the π–π stacking distance ($d_{\pi-\pi}$), the density (ρ), the potential energy of the optimized geometry with respect to the lowest optimized potential energy starting from different α_0, the α values obtained from experimental X-ray diffraction studies and other calculations, HOMO (LUMO) intermolecular transfer integrals t_{HOMO} (t_{LUMO}) calculated at both INDO and DFT levels. Different α_0 may go to the same α after geometry optimization, thus all α_0 values are provided. The values between parentheses denote absolute tilt angles between the thiophene rings and the substrate.

A	α_0 [°][a)]	α [°]	*a*/5 [Å]	*b* [Å]	*c*/5 [Å]	S-C-C-S dihedral angle [°]	C=C–C–C dihedral angle [°]	$d_{\pi-\pi}$ [Å]	ρ [g cm^{-3}]	ΔE [kcal mol^{-1}]	Exp. α [°]	Calc. α [°]	t_{HOMO} [eV] INDO	t_{LUMO} [eV] INDO	t_{HOMO} [eV] DFT	t_{LUMO} [eV] DFT
4	60–80; 110–120	67 (67)	12.73	7.60	7.85	1.1	86.1	3.50	1.21	0	84°[b)]		0.172	0.027	0.154	0.050
	85–105	93 (87)	14.20	7.34	7.85	6.1	103.0	3.66	1.12	20.5			0.112	0.129	0.103	0.216
6	60–65	67 (67)	16.82	7.53	7.85	0.7	85.0	3.46	1.11	2.2	60°–62°,[51] 64[52]	83[56]	0.184	0.029	0.162	0.052
	70–115	89 (89)	17.20	7.16	7.84	5.6	102.8	3.58	1.14	0	85°[50]		0.135	0.163	0.119	0.252
8	60–65	68 (68)	19.37	7.36	7.83	0.5	84.3	3.41	1.16	5.4			0.194	0.015	0.170	0.072
	70–85	81 (81)	20.86	7.15	7.85	4.3	96.7	3.53	1.10	0	84°[50]		0.156	0.130	0.136	0.219
	95–105	95 (85)	20.01	7.18	7.85	3.7	112.5	3.58	1.14	5.4			0.120	0.145	0.106	0.236

[a)]Thiophene tilt angles α_0 in initial P3*A*T geometries were varied in steps of 5° for the given ranges. For instance, α_0 values of 60, 65, 70, 75, and 80 were used for the range 60–80°; [b)]Form I' as described elsewhere.[54]

Since crystals with distinct α values and close potential energies are observed for the same polymer, the calculations suggest that these could yield different domains that coexist in real samples. The relative energies for the various crystal structures identified from the MM calculations (see Table 4) then indicate that α should increase from P34T to P36T, suggesting that part of the observed variation in $<\alpha>$ at the polymer/air interface could be due to the presence of different polymorphs with different α_{cryst}. An alternative explanation for the increase of $<\alpha>$ in going from P34T to P36T and P37T could be due to an increase in structural order within the top layer. In that respect it is noteworthy that from a combined TEM, AFM, XRD and UV-Vis spectroscopy study to the order within crystalline P3*A*T NFs it was deduced that the order strongly increases when going from P33T to P35T, while for longer alkyl side chains it improved only marginally.[32] Also structural disorder at domain boundaries could reduce $<\alpha>$, since the NF widths w_{NF} show a similar trend as that of $<\alpha>$ (Table 3). Such a correlation is, however, not observed for the nodule width w_n and $<\alpha>$ of the CB-P3*A*T/air interface.

Altogether, the calculations and literature data so far suggest that the observed tilt angles at the CB- and NF-P3*A*T/air interfaces in the range 64.4–69.1° could indeed be due to highly ordered structures with near-crystalline thiophene setting angles that are close to 70°, although a combination of (more) disorder and higher setting angles, above 80° cannot be totally excluded. With the optimized crystal structures in hand, we can proceed by calculating the electronic transfer integrals mediating charge transport and comparing them with the measured mobilities.

2.5.2. Electronic Structure and Transfer Integrals

On the basis of the different polymorphs identified from the molecular mechanics simulations, we calculated the intermolecular transfer integrals for adjacent polymer chains, as extracted from the MM crystal structures. The intermolecular transfer integral t is a parameter that governs the rate of charge transfer between two molecules and hence the charge mobilities.[58,59] This parameter reflects the strength of the interactions between the electronic wavefunctions of two adjacent molecules. When applied to the HOMO [LUMO] level, it measures the ease of hole [electron] transport. The intermolecular transfer integrals are known to be very sensitive to the relative positions of the molecules[60] and hence are expected to vary for the different polymorphs. Here, the electronic transfer integrals were computed at both the INDO (intermediate neglect of differential overlap) and DFT levels (using the B3LYP functional with a double zeta basis set).[61,62] Note that, in both sets of quantum-chemical calculations, we only considered thiophene hexamers and replaced the long alkyl chains by a methyl group since the alkyl chains are not expected to modify the energy and shape of the frontier electronic orbitals.

The calculated HOMO and LUMO intermolecular transfer integrals are listed in Table 4 for all possible structures. Both INDO and DFT results show that the transfer integrals vary significantly with the crystal structure and (therefore) alkyl chain length. The effect is particularly pronounced for electrons where changes in electronic couplings by up to one order of magnitude are predicted for different α values. As a result, the relative values of t_{HOMO} and t_{LUMO} depend very much on the structure: namely, while all P3*A*Ts exhibit a much larger HOMO than LUMO intermolecular transfer integral for the small tilt angle structure, the opposite situation holds true at larger tilt angles.

In a hopping regime, the mobility should scale with the squared transfer integral for disorder-free and defect-free systems.[58] From the INDO values in Table 4 it can be deduced that t^2_{HOMO} splits up in two sets of about $(3.4 \pm 0.4) \times 10^{-2}$ and $(1.7 \pm 0.5) \times 10^{-2}$ eV^2 for the structures with α_{cryst} of 67–68° and 81–89°, respectively. The fact that the mobilities that we measure at the polymer/air interface do not change significantly with alkyl chain length hints to more or less identical α_{cryst} values for the different polymers, although care must be taken here, given the fact that the variation of t^2_{HOMO} with α_{cryst} is only a factor of 2 and the fact that the mobility values that we measure are limited by extrinsic factors such as grain boundaries or structural disorder in general,[63] and can thus differ significantly from the theoretical values calculated for ideal systems.

2.6. General Discussion

Based on experimental results on P3*A*Ts,[3,8,11] the thiophene tilt angle $<\alpha>$ as obtained from NEXAFS is commonly interpreted as an average between oop and ip oriented crystallites at the interface.[25,45] In **Figure 4** we have plotted the FET mobilities as a function of $<\alpha>$ of the spin-coated layers for each interface (CB-P3*A*T/SiO_2,[26] NF-P3*A*T/SiO_2,[26] CB-P3*A*T/air). Note that the mobilities of the CB-P3*A*T/air interface were measured on a bare SiO_2 gate, after flipping the film. Even though the variation in alkyl chain length may lead to some variation in the crystalline setting angle α_{cryst} (vide supra), it is clear that μ_{FET} is a strong function of the (average) polymer orientation at the interface as contained in $<\alpha>$ and that the highest oop orientation corresponds with the highest mobilities. The change of interface from SiO_2 to air induces a huge change in mobility

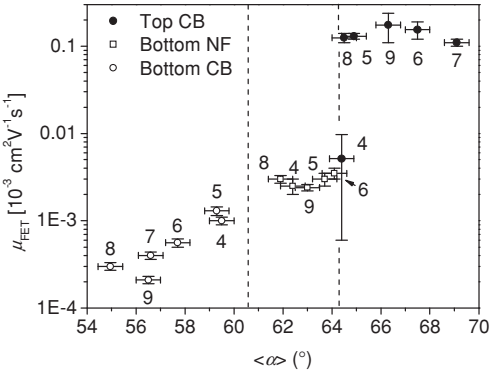

Figure 4. FET mobilities for bottom gate FETs of P3*A*T layers from CB deposited on bare SiO_2 (left, "Bottom CB"), P3*A*T NF layers deposited on bare SiO_2 (center, "Bottom NF") and P3*A*T films from CB that were reversed and transferred to a SiO_2 gate dielectric such that the original polymer/air interface faces the SiO_2 (right, 'Top CB'). For each point *A* has been indicated.

of 1 to 3 orders of magnitude, while it has only a modest effect on <α>. It appears that a very small population of ip oriented P3*A*T can have a dramatic impact on hole mobility. When the <α> values obtained at the CB-P3*A*T/air interface are taken as 100% oop oriented P3*A*T, it can be estimated (Table 3) that at the CB-P3*A*T/SiO_2 interface, depending on *A*, 8 to 18% of the polymer has the "wrong" ip orientation as far as hole mobility is concerned. For the NF-P3*A*T/SiO_2 interface, this is only 1.8 to 5%. But even this estimated 1.8% ip oriented P35T reduces the hole mobility with more than 1 order of magnitude. While obviously not all morphological differences between the two interfaces can be captured in <α>, these results emphasize the huge impact that small amounts of ip oriented P3*A*T can have on hole mobility. Note that the vertical dashed lines in Figure 4 are just guides to the eye and do not imply any definite boundaries at the corresponding <α> values.

The fact that highest FET mobilities are obtained at the interface with air is in line with the results of Veres,[14] Grecu,[15] and Tomatsu[64] on bottom gate P36T FETs on gate dielectrics of different polarity. They observed an increase of the FET mobility with increasing water contact angle (decreasing surface energy) of the gate dielectric. Since the water contact angle of freshly UV-ozone cleaned SiO_2 is in the range 0–5° and the theoretical water contact angle of air or N_2 should be 180°, the mobilities obtained at the P3*A*T/SiO_2 and P3*A*T/air interfaces can be positioned at both extremes of the polarity scale. It explains the large orienting effect that air or N_2 has during surface structure formation and suggests a general method to achieve high oop orientations and high FET mobilities for hairy comb type semiconducting polymers, similar in approach to what is attempted with superhydrophobic gate dielectrics.[65] In this respect it should be noted that although we have only tested chlorobenzene as a solvent, the high tilt angles obtained by Hao et al.[39] suggest that a lower boiling point solvent like chloroform can be used equally well, provided that conditions of slow drying are applied (possibly in combination with thermal annealing). Our results also shed light on the issue of top gate FETs often displaying relatively high mobilities.

3. Conclusions

We have demonstrated relatively high and alkyl chain length independent FET mobilities of 0.14 ± 0.03 $cm^2\ V^{-1}\ s^{-1}$ for bottom gate FETs of P3*A*T films that were spin-coated from CB and flipped such that the original polymer/air interface faces the bare SiO_2 gate dielectric. These mobilities were almost 2 orders of magnitude higher than those previously obtained for NFs of the same polymers spin-coated directly on bare SiO_2 and 2 to 3 orders of magnitude higher than those previously obtained for CB spin-coated films on bare SiO_2. By means of TEY NEXAFS of the polymer/air interfaces of the spin-coated NF- and CB-P3*A*T films very high and almost identical levels of oop oriented P3*A*T were found, much higher than previously obtained at the SiO_2 interface. The NEXAFS results on both CB- and NF-P3*A*T/air interfaces suggest that the found average thiophene tilt angle range of 64.4–69.1° represents close to crystalline oop orientation levels. This was supported with molecular mechanics calculations on ideal P3*A*T crystals in combination with the calculation of transfer integrals for those crystals. On the basis of our results, however, a combination of more disorder and higher crystalline setting angles (>80°) cannot be totally excluded. Finally, our results suggest that a very small fraction of wrongly oriented polymer can have a huge negative impact on charge carrier mobility and furthermore highlight the possibility of achieving excellent oop orientation for hairy comb type polymers like P3*A*T at the interface with air.

4. Experimental Section

The synthesis, purification and characterization of the P3*A*Ts used in this study and the preparation of the NF dispersions has been reported elsewhere.[32] Layer thicknesses have been reported in the literature.[26]

FET and NEXAFS Sample Preparation: The FET substrates (obtained from Philips) contained heavily doped Si with a conductivity of (0.2 to 1) × 10^3 S cm^{-1} as the gate electrode. A 204 nm thick layer of SiO_2 with a unit area capacitance of 16.9 nF cm^{-2} acted as the gate dielectric. The source and drain electrodes consisted of Au (100 nm) on top of Ti (10 nm). Prior to deposition of the polymer layer, the substrate was cleaned using a standard procedure (20 min ultrasound in soap, 10 min ultrasound in acetone, 10 min in boiling isopropanol, 15 min of UV-ozone to remove the HDMS layer, which is present on the SiO_2 gate dielectric of the commercial FET substrates).

For NEXAFS, doped Si substrates with a ≈200 nm thick SiO_2 layer were used. The SiO_2 layer was removed by immersing the substrate in 40% HF solution for 20 min, followed by extensive rinsing with 18 MΩ water. The substrates were then cleaned (and re-oxidized) as described for the FET substrates prior to depositing the polymer layer.

Polymers were dissolved in CB (1 wt% for NEXAFS, 2 wt% for FET) at 120 °C and filtered through a 0.45 µm pore size PTFE filter. The solutions stirred at 120 °C for minimally 15 min. were cooled down to 50 °C just before spin-coating at 2000 rpm (60 s). The P34T solution was cooled down only to 100 °C (NEXAFS) or spun from 90 °C (FET) to prevent aggregation. NF dispersions (0.4 to 0.6 wt%) were spin-coated at 1000 rpm (120 s) after stirring for several days at room temperature. In all cases an acceleration of 500 rpm s^{-1} was used. All layers were allowed to dry overnight until all solvent had evaporated before proceeding. For FET the films were flipped as described in Section 2.2.

Field-Effect Transistor Measurements: Current–voltage characteristics were measured using two Keithley 2400 source meters. On/off ratios were determined at a field of 0.1 MV m^{-1} (linear regime) and V_G = –50 V. The mobility was then obtained from a fit of the linear region of the transfer characteristic (Figure 2c) at small V_D. Each mobility value was measured for at least 4 channel lengths varying between 10 and 40 µm. The channel width was 10 or 20 mm. Light was excluded from the samples at least 15 min before and during the measurements since it was found to influence the results. The values obtained in this way were very reproducible. All FET preparation and measurements were performed under N_2 atmosphere.

AFM Measurements: Experimental details have been given before.[26] Typical fiber and domain sizes were extracted by dividing the AFM phase image (500 nm × 500 nm for CB-P3*A*T layers and 1 µm × 1 µm for NF-P3*A*T layers) in 10 equal rows in which at 5 points for each row the fiber or nodule width was determined visually. Average values are given.

NEXAFS Measurements: NEXAFS measurements were performed at the Soft X-Ray (SXR) Apple II undulator beamline at the Australian Synchrotron.[66] The undulator was set up to output horizontal polarized light that was then monochromatized using a Peterson plane grating monochromator (PGM) with a grating of 1200 lines mm^{-1}. An ultrahigh vacuum (UHV) chamber, which had a base pressure of 2 × 10^{-10} mbar, was attached to the end of the beam line. Total electron yield (TEY) carbon *K*-edge NEXAFS spectra were collected by grounding the substrate and measuring the sample-to-ground current that corresponds

to the total intensity of photoelectrons that are excited from core levels into unoccupied states above the Fermi level. A clean sputtered Au sample was used as a reference and the raw spectra were normalized as discussed by Watts et al.[67] The energy resolution at the carbon *K*-edge is approximately 30 meV with an exit slit of 20 mm and a C_{ff} (constant fixed focus) value of 2. The photon flux is 3×10^{11} photons s^{-1} (with a storage ring current of 200 mA) and the spot size was approximately 0.6 × 0.6 mm however the spot was deliberately ''defocused'' to minimize beam damage of the samples. The effects of radiation damage were assessed by repeating the same measurement on the same spot of the substrate for a significant period of time in order to produce changes in the normed carbon *K*-edge structure. Once the period of time to produce beam damage on a sample was known scan parameters were chosen to minimize this. Furthermore the beam was moved to a fresh spot of the film in between each sample scan, allowing the recording of subsequent measurements to be collected for this manuscript with negligible beam damage. Likewise, no sample charging was observed. It is well-established that the molecular orientation of adsorbates on substrates can be determined from polarization-dependent NEXAFS spectra obtained at various angles in relation to the substrate surface.[42] In this manuscript carbon *K*-edge spectra were recorded at angles of 20°, 55°, and 90° measured between the direction vector of the incident linear polarized light and the surface plane of the sample (meaning that for an angle of 90° the electric field vector, ***E***, will be parallel to the surface plane, whereas at 20° ***E*** will be almost perpendicular to the surface plane). The π^* resonance at 284.5 eV within the NEXAFS spectra was identified and fitted with Gaussian peaks to find the integrated intensity areas (*I*) under the resonance and the orientation of the thiophene units with respect to the substrate were determined according to

$$I = 1 + \left(3\cos^2\theta - 1\right)\left(3\cos^2 < \alpha > -1\right) \quad (1)$$

where θ is the angle of incidence of the X-ray beam and $<\alpha>$ is the average tilt angle.[42]

Theoretical Calculations: The force field parameters for the Molecular Mechanics calculations were obtained from the standard OPLS-AA force field database except the following: 1) The atomic charges of the thiophenes were calculated from the central thiophene ring in 2,2′:5′,2″-terthiophene at the MP2/aug-cc-pVTZ level, based on the fully optimized geometry at the computationally less expensive MP2/cc-pVDZ level. These charges are shown in the inset of **Figure 5**. 2) The torsional potential between the thiophene rings was taken from previous ab initio studies on 2,2′-bithiophene using MP2/aug-cc-pVTZ (see Figure 5).[68] 3) The torsional potential between one thiophene ring and an alkane chain was calculated at the same level on 3-ethylthiophene in the present study. As shown in Figure 5, constrained optimizations with C–C–C–C dihedral angle fixed at ϕ = 0°, 15°, 30°, ..., 360° were performed first. Starting from the optimized structure with the lowest energy, an additional full optimization was then carried out to get the global minimum of the potential energy curve. Afterwards, an interpolation on these discrete data points by a truncated Fourier expansion $\Delta E(\phi) = V_0 + \sum_{i=1}^{6} V_i \cos(i\pi\phi/180)$ was made and further used to build up the force field. 4) The bond stretching and the bond angle bending were described by harmonic potentials using the MM3 force field.[69,70] Note that all the ab initio calculations in this work were performed with the Gaussian 03 package.[71]

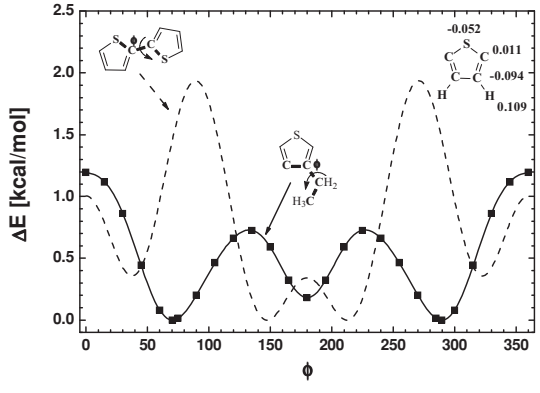

Figure 5. Calculated torsional potential of 2,2′-bithiophene (dash)[68] and 3-ethylthiophene (solid) at the MP2/aug-cc-pVTZ level. The squares represent the torsions which are explicitly calculated ab initio in this study. The calculated atomic charge distribution in the thiophene ring is also shown (top right corner).

In the crystal structure optimizations both the atomic coordinates and the lattice parameters were optimized through the XTALMIN program within TINKER 5.1 molecular modeling package.[72]

INDO Transfer Integrals: were computed by expanding the molecular orbitals ϕ_1 and ϕ_2 of the two interacting molecules into atomic contributions:[73]

$$t = \langle\phi_1|h|\phi_2\rangle = \sum_{\mu}\sum_{\upsilon} C_{1\mu}C_{2\upsilon}\langle\chi_\mu|h|\chi_\upsilon\rangle \quad (2)$$

where $C_{1\mu}$ (C_{2v}) corresponds to the LCAO (linear combination of atomic orbital) coefficients of the atomic orbital χ_μ (χ_v) in the molecular orbital ϕ_1 (ϕ_2). The matrix element $\langle\chi_\mu|h|\chi_\upsilon\rangle$ is implemented in the INDO method as:

$$\langle\chi_\mu|h|\chi_\upsilon\rangle = \frac{1}{2}(\beta_A + \beta_B)\,\bar{S}_{\mu\upsilon} \quad (3)$$

where β_A and β_B are two parameters depending on the chemical nature of atoms A and B, and $\bar{S}_{\mu\upsilon}$ is the overlap factor between the atomic orbitals χ_μ and χ_v corrected by empirical factors.[74]

DFT-Calculated (B3LYP/DZ) Transfer Integrals:[61,62,75] Polarization effects can create an offset between the electronic levels of the molecules in the dimer. Such a contribution that overestimates the transfer integral is taken into account trough the estimates of the site energies ε_j. In practice, within the fragment orbital approach implemented in the ADF package,[76] the orbitals of the dimers are obtained by solving the Kohn-Sham equation using the molecular orbitals of the fragments as a basis set. The site energies ε_j and coupling elements t_{ij} are then obtained from the energies of the molecular orbitals of the individual fragments in the dimer:

$$\varepsilon_j = \langle\phi_j^{\mathrm{HOMO}}|\hat{H}|\phi_j^{\mathrm{HOMO}}\rangle \quad (4)$$

$$t_{ij} = \langle\phi_j^{\mathrm{HOMO}}|\hat{H}|\phi_j^{\mathrm{HOMO}}\rangle \quad (5)$$

Since the orbitals of the individual fragments are not orthogonal, an orthogonalization (or Löwdin) transformation is applied to the Kohn-Sham matrix to ensure invariance of the transfer integrals with respect to the choice of the energy origin. The invariant transfer integrals (t) then write:

$$t = \frac{t_{ij} - 0.5\left(\varepsilon_i + \varepsilon_j\right)S_{ij}}{1 - S_{ij}^2} \quad (6)$$

where ε_{ij}, t_{ij}, and S_{ij} are the diagonal and non-diagonal elements of the Kohn-Sham matrix and the non-diagonal elements of the overlap matrix.

Acknowledgements

Dr. Koen Vandewal and Dr. Abay Gadisa are acknowledged for valuable discussions. This work was partly supported by the Engineering and Physical Sciences Research Council UK (EP/E051804/1). Part of this research was undertaken on the soft X-ray beamline at the Australian Synchrotron, Victoria, Australia. The research in Mons has been partly

supported by the European Commission through the project ONE-P (NMP3-LA-2008-212311) and SUPERIOR (ITN-238177), by Région Wallonne (FEDER – Smartfilm RF project and the OPTI2MAT excellence program). DB is FNRS Research Director. Furthermore, the authors acknowledge financial support from the INTERREG project ORGANEXT and from The Fund for Scientific Research-Flanders (FWO) and the BELSPO in the frame of the network IAP P6/27. The authors also thank the IWT (Institute for the Promotion of Innovation by Science and Technology in Flanders) for financial support via the SBO project "Polyspec".

Received: September 24, 2013
Published online: November 27, 2013

[1] A. C. Arias, J. D. MacKenzie, I. McCulloch, J. Rivnay, A. Salleo, *Chem. Rev.* **2010**, *110*, 3.
[2] I. McCulloch, M. Heeney, M. L. Chabinyc, D. M. DeLongchamp, R. J. Kline, M. Cölle, W. Duffy, D. Fischer, D. Gundlach, B. Hamadani, R. Hamilton, L. Richter, A. Salleo, M. Shkunov, D. Sparrowe, S. Tierney, W. Zhang, *Adv. Mater.* **2009**, *21*, 1091.
[3] H. Sirringhaus, P. J. Brown, R. H. Friend, M. M. Nielsen, K. Bechgaard, B. M. W. Langeveld-Voss, A. J. H. Spiering, R. A. J. Janssen, E. W. Meijer, P. Herwig, D. M. de Leeuw, *Nature* **1999**, *401*, 685.
[4] G. Wang, J. Swensen, D. Moses, A. J. Heeger, *J. Appl. Phys.* **2003**, *93*, 6137.
[5] H. Yang, J. S. Shin, K. Cho, C. Y. Ryu, Z. Bao, *Adv. Funct. Mater.* **2005**, *15*, 671.
[6] M. Surin, P. Leclère, R. Lazzaroni, J. D. Yuen, G. Wang, D. Moses, A. J. Heeger, S. Cho, K. Lee, *J. Appl. Phys.* **2006**, *100*, 033712.
[7] R. Zhang, B. Li, M. C. Iovu, M. Jeffries-EL, G. Sauvé, J. Cooper, S. Jia, S. Tristam-Nagle, D. M. Smilgies, D. N. Lambeth, R. D. McCullough, T. Kowalewski, *J. Am. Chem. Soc.* **2006**, *128*, 3480.
[8] J.-F. Chang, J. Clark, N. Zhao, H. Sirringhaus, D. W. Breiby, J. W. Andreasen, M. M. Nielsen, M. Giles, M. Heeney, I. McCulloch, *Phys. Rev. B: Condens. Matter* **2006**, *74*, 115318.
[9] E. J. Samuelsen, J. Mårdalen, in *Handbook of Organic Conductive Molecules and Polymers*, Vol. *3*. Conductive Polymers: Spectroscopy and Physical Properties. (Ed: H. S. Nalwa), John Wiley & Sons Ltd, Chichester **1997**, 87.
[10] M. J. Winokur, in *Handbook of Conducting Polymers, Theory, Synthesis, Properties, and Characterization*, (Eds: T. A. Skotheim, J. R. Reynolds), CRC Press, Boca Raton **2007**.
[11] K. E. Aasmundtveit, E. J. Samuelsen, M. Guldstein, C. Steinsland, O. Flornes, C. Fagermo, T. M. Seeberg, L. A. A. Pettersson, O. Inganas, R. Feidenhans'l, S. Ferrer, *Macromolecules* **2000**, *33*, 3120.
[12] Y. D. Park, J. A. Lim, H. S. Lee, K. Cho, *Mater. Today* **2007**, *10*, 46.
[13] X. N. Sun, C. A. Di, Y. Q. Liu, *J. Mater. Chem.* **2010**, *20*, 2599.
[14] J. Veres, S. Ogier, G. Lloyd, D. de Leeuw, *Chem. Mater.* **2004**, *16*, 4543.
[15] S. Grecu, M. Roggenbuck, A. Opitz, W. Brütting, *Org. Electron.* **2006**, *7*, 276.
[16] D. H. Kim, Y. D. Park, Y. S. Jang, H. C. Yang, Y. H. Kim, J. I. Han, D. G. Moon, S. J. Park, T. Y. Chang, C. W. Chang, M. K. Joo, C. Y. Ryu, K. W. Cho, *Adv. Funct. Mater.* **2005**, *15*, 77.
[17] A. Babel, S. A. Jenekhe, *J. Phys. Chem. B* **2003**, *107*, 1749.
[18] M. Xu, K. Nagai, M. Nakamura, K. Kudo, M. Iizuka, *Appl. Phys. Lett.* **2007**, *90*, 223512.
[19] A. Babel, S. A. Jenekhe, *Synth. Meth.* **2005**, *148*, 169.
[20] J. Paloheimo, H. Stubb, P. Yli-Lahti, P. Kuivalainen, *Synth. Meth.* **1991**, *41*, 563.
[21] K. Kaneto, W. Y. Lim, W. Takashima, T. Endo, M. Rikukawa, *Jpn. J. Appl. Phys., Part 2* **2000**, *39*, L872.
[22] Y. D. Park, D. H. Kim, Y. Jang, J. H. Cho, M. Hwang, H. S. Lee, J. A. Lim, K. Cho, *Org. Electron.* **2006**, *7*, 514.
[23] R. J. Kline, M. D. McGehee, M. F. Toney, *Nat. Mater.* **2006**, *5*, 222.
[24] C. C. Wang, L. H. Jimison, L. Goris, I. McCulloch, M. Heeney, A. Ziegler, A. Salleo, *Adv. Mater.* **2010**, *22*, 697.
[25] R. J. Kline, D. M. DeLongchamp, D. A. Fischer, E. K. Lin, M. Heeney, I. McCulloch, M. F. Toney, *Appl. Phys. Lett.* **2007**, *90*.
[26] W. D. Oosterbaan, J. C. Bolsée, A. Gadisa, V. Vrindts, S. Bertho, J. D'Haen, T. J. Cleij, L. Lutsen, C. R. McNeill, L. Thomsen, J. V. Manca, D. Vanderzande, *Adv. Funct. Mater.* **2010**, *20*, 792.
[27] S. Samitsu, T. Shimomura, S. Heike, T. Hashizume, K. Ito, *Macromolecules* **2010**, *43*, 7891.
[28] B. S. Ong, Y. Wu, P. Liu, S. Gardner, *J. Am. Chem. Soc.* **2004**, *126*, 3378.
[29] M. L. Chabinyc, A. Salleo, Y. Wu, P. Liu, B. S. Ong, M. Heeney, I. McCulloch, *J. Am. Chem. Soc.* **2004**, *126*, 13928.
[30] Y. H. Kim, J. I. Han, D. G. Moon, *J. Korean Phys. Soc.* **2006**, *48*, S118.
[31] Q. Wei, S. Miyanishi, K. Tajima, K. Hashimoto, *ACS Appl. Mater. Interfaces* **2009**, *1*, 2660.
[32] W. D. Oosterbaan, V. Vrindts, S. Berson, S. Guillerez, O. Douhéret, B. Ruttens, J. D'Haen, P. Adriaensens, J. Manca, L. Lutsen, D. Vanderzande, *J. Mater. Chem.* **2009**, *19*, 5424.
[33] R. J. Kline, M. D. McGehee, E. N. Kadnikova, J. S. Liu, J. M. J. Frechet, *Adv. Mater.* **2003**, *15*, 1519.
[34] A. Zen, J. Pflaum, S. Hirschmann, W. Zhuang, F. Jaiser, U. Asawapirom, J. P. Rabe, U. Scherf, D. Neher, *Adv. Funct. Mater.* **2004**, *14*, 757.
[35] S. Hoshino, M. Yoshida, S. Uemura, T. Kodzasa, N. Takada, T. Kamata, K. Yase, *J. Appl. Phys.* **2004**, *95*, 5088.
[36] Y. M. Sun, X. F. Lu, S. W. Lin, J. Kettle, S. G. Yeates, A. M. Song, *Org. Electron.* **2010**, *11*, 351.
[37] P.-T. Wu, H. Xin, F. S. Kim, G. Ren, S. A. Jenekhe, *Macromolecules* **2009**, *42*, 8817.
[38] G. Sauve, A. E. Javier, R. Zhang, J. Y. Liu, S. A. Sydlik, T. Kowalewski, R. D. McCullough, *J. Mater. Chem.* **2010**, *20*, 3195.
[39] X. T. Hao, T. Hosokai, N. Mitsuo, S. Kera, K. K. Okudaira, K. Mase, N. Ueno, *J. Phys. Chem. B* **2007**, *111*, 10365.
[40] J. Rivnay, L. H. Jimison, M. F. Toney, M. Preiner, N. A. Melosh, A. Salleo, *J. Vac. Sci. Technol., B* **2008**, *26*, 1454.
[41] Y. Jung, R. J. Kline, D. A. Fischer, E. K. Lin, M. Heeney, I. McCulloch, D. M. Delongchamp, *Adv. Funct. Mater.* **2008**, *18*, 742.
[42] J. Stöhr, *NEXAFS Spectroscopy*, Vol. *25* of Springer Series in Surface Sciences (Eds: G. Ertl, R. Gomer, D. L. Mills), Springer, Berlin **1996**.
[43] A. P. Hitchcock, J. A. Horsley, J. Stöhr, *J. Chem. Phys.* **1986**, *85*, 4835.
[44] D. M. DeLongchamp, B. M. Vogel, Y. Jung, M. C. Gurau, C. A. Richter, O. A. Kirillov, J. Obrzut, D. A. Fischer, S. Sambasivan, L. J. Richter, E. K. Lin, *Chem. Mater.* **2005**, *17*, 5610.
[45] P. K. H. Ho, L. L. Chua, M. Dipankar, X. Y. Gao, D. C. Qi, A. T. S. Wee, J. F. Chang, R. H. Friend, *Adv. Mater.* **2007**, *19*, 215.
[46] L. L. Chua, M. Dipankar, S. Sivaramakrishnan, X. Y. Gao, D. C. Qi, A. T. S. Wee, P. K. H. Ho, *Langmuir* **2006**, *22*, 8587.
[47] G. Horowitz, *J. Mater. Res.* **2004**, *19*, 1946.
[48] K. J. Ihn, J. Moulton, P. Smith, *J. Polym. Sci., Part B: Polym. Phys.* **1993**, *31*, 735.
[49] S. Berson, R. De Bettignies, S. Bailly, S. Guillerez, *Adv. Funct. Mater.* **2007**, *17*, 1377.
[50] T. J. Prosa, M. J. Winokur, J. Moulton, P. Smith, A. J. Heeger, *Macromolecules* **1992**, *25*, 4364.
[51] K. Tashiro, M. Kobayashia, S. Morita, T. Kawai, K. Yoshino, *Synth. Meth.* **1995**, *69*, 397.
[52] N. Kayunkid, S. Uttiya, M. Brinkmann, *Macromolecules* **2010**, *43*, 4961.
[53] W. L. Jorgensen, D. S. Maxwell, J. Tirado-Rives, *J. Am. Chem. Soc.* **1996**, *118*, 11225.
[54] P. Arosio, M. Moreno, A. Famulari, G. Raos, M. Catellani, S. V. Meille, *Chem. Mater.* **2009**, *21*, 78.

[55] S. Chambon, W. D. Oosterbaan, R. Mens, J. D'Haen, L. Lutsen, D. Vanderzande, P. Adriaensens, unpublished.
[56] A. Maillard, A. Rochefort, *Phys. Rev. B: Condens. Matter Mater. Phys.* **2009**, *79*, 115207.
[57] B. Meredig, A. Salleo, R. Gee, *ACS Nano* **2009**, *3*, 2881.
[58] V. Coropceanu, J. Cornil, D. A. da Silva Filho, Y. Olivier, R. Silbey, J.-L. Brédas, *Chem. Rev.* **2007**, *107*, 926.
[59] V. Lemaur, S. Bouzakraoui, Y. Olivier, P. Brocorens, C. Burhin, J. E. Beghdadi, A. Martin-Hoyas, A. M. Jonas, D. A. Serban, A. Vlad, N. Boucher, J. Leroy, M. Sferrazza, P.-O. Mouthuy, S. Melinte, S. Sergeev, Y. Geerts, R. Lazzaroni, J. Cornil, B. Nysten, *J. Phys. Chem. C* **2010**, *114*, 4617.
[60] V. Lemaur, D. A. da Silva Filho, V. Coropceanu, M. Lehmann, Y. Geerts, J. Piris, M. G. Debije, A. M. van de Craats, K. Senthilkumar, L. D. A. Siebbeles, J. M. Warman, J.-L. Brédas, J. Cornil, *J. Am. Chem. Soc.* **2004**, *126*, 3271.
[61] E. F. Valeev, V. Coropceanu, D. A. da Silva Filho, S. Salman, J.-L. Brédas, *J. Am. Chem. Soc.* **2006**, *128*, 9882.
[62] L. Viani, Y. Olivier, S. Athanasopoulos, D. A. da Silva Filho, J. Hulliger, J.-L. Brédas, J. Gierschner, J. Cornil, *ChemPhysChem* **2010**, *11*, 1062.
[63] J. F. Chang, H. Sirringhaus, M. Giles, M. Heeney, I. McCulloch, *Phys. Rev. B* **2007**, *76*.
[64] K. Tomatsu, T. Hamada, T. Nagase, S. Yamazaki, T. Kobayashi, S. Murakami, K. Matsukawa, H. Naito, *Jpn. J. Appl. Phys.* **2008**, *47*, 3196.
[65] J.-H. Park, S.-J. Kang, J.-W. Park, B. Lim, D.-Y. Kima, *Appl. Phys. Lett.* **2007**, *91*, 222108.
[66] B. C. C. Cowie, A. Tadich, L. Thomsen, "The Current Performance of the Wide Range (90-2500 eV) Soft X-ray Beamline at the Australian Synchrotron", presented at *SRI 2009, The 10th International Conference on Synchrotron Radiation Instrumentation*, Melbourne (Australia), **2009**.
[67] B. Watts, L. Thomsen, P. C. Dastoor, *J. Electron. Spectrosc. Relat. Phenom.* **2006**, *151*, 105.
[68] G. Raos, A. Famulari, V. Marcon, *Chem. Phys. Lett.* **2003**, *379*, 364.
[69] N. L. Allinger, Y. H. Yuh, J. H. Lii, *J. Am. Chem. Soc.* **1989**, *111*, 8551.
[70] V. Marcon, G. Raos, *J. Am. Chem. Soc.* **2006**, *128*, 1408.
[71] M. J. Frisch, G. W. Trucks, H. B. Schlegel, G. E. Scuseria, M. A. Robb, J. R. Cheeseman, J. Montgomery, J. A. Montgomery, Jr., T. Vreven, K. N. Kudin, J. C. Burant, J. M. Millam, S. S. Iyengar, J. Tomasi, V. Barone, B. Mennucci, M. Cossi, G. Scalmani, N. Rega, G. A. Petersson, H. Nakatsuji, M. Hada, M. Ehara, K. Toyota, R. Fukuda, J. Hasegawa, M. Ishida, T. Nakajima, Y. Honda, O. Kitao, H. Nakai, M. Klene, X. Li, J. E. Knox, H. P. Hratchian, J. B. Cross, V. Bakken, C. Adamo, J. Jaramillo, R. Gomperts, R. E. Stratmann, O. Yazyev, A. J. Austin, R. Cammi, C. Pomelli, J. W. Ochterski, P. Y. Ayala, K. Morokuma, G. A. Voth, P. Salvador, J. J. Dannenberg, V. G. Zakrzewski, S. Dapprich, A. D. Daniels, M. C. Strain, O. Farkas, D. K. Malick, A. D. Rabuck, K. Raghavachari, J. B. Foresman, J. V. Ortiz, Q. Cui, A. G. Baboul, S. Clifford, J. Cioslowski, B. B. Stefanov, G. Liu, A. Liashenko, P. Piskorz, I. Komaromi, R. L. Martin, D. J. Fox, T. Keith, M. A. Al-Laham, C. Y. Peng, A. Nanayakkara, M. Challacombe, P. M. W. Gill, B. Johnson, W. Chen, M. W. Wong, C. Gonzalez, J. A. Pople, *Gaussian 03*, **2004**, Gaussian, Inc., Wallingford CT.
[72] J. W. Ponder, *TINKER: Software Tools for Molecular Design*, Washinton University School of Medicine, Saint Louis, MO **2003**.
[73] A. Van Vooren, J.-S. Kim, J. Cornil, *ChemPhysChem* **2008**, *9*, 989.
[74] J. Ridley, M. Zerner, *Theor. Chim. Acta* **1973**, *32*, 111.
[75] J. C. Sancho-García, A. J. Pérez-Jiménez, Y. Olivier, J. Cornil, *Phys. Chem. Chem. Phys.* **2010**, *12*, 9381.
[76] *ADF2010.01*, SCM, Theoretical Chemistry, Vrije Universiteit, Amsterdam, The Netherlands, http://www.scm.com (accessed: September, 2013).